

Evaluation of crystalline structure and SO₂ storage capacity of a series of composition-sensitive De-SO₂ catalysts

J.A. Wang^{a,*}, L.F. Chen^a, R. Limas-Ballesteros^a, A. Montoya^b, J.M. Dominguez^b

^a Superior School of Chemical Engineering and Industrial Extraction (ESIQIE), National Polytechnic Institute (IPN), Col. Zacatenco, 07738 Mexico City, Mexico

^b Instituto Mexicano del Petróleo, Grupo de Simulación Molecular, Eje Central Lázaro Cárdenas No. 152, Delegación G.A. Madero, 07730 México DF, Mexico

Received 9 May 2002; accepted 22 August 2002

Abstract

A series of non-stoichiometric magnesium-aluminate solid solution spinels, used as sulfur-transfer catalysts in the fluid catalytic cracking units for SO_x emissions abatement, were prepared by using coprecipitation method and characterized with BET, TGA, AES, XRD and in situ IR techniques. It was found that both the crystalline structures and De-SO_x activities of magnesium-aluminate spinels are very sensitive to catalyst compositions. Several phase domains were produced by changing the mole ratio of alumina to magnesia in the preparation process. Owing to substitution of magnesium or aluminum ions in the spinel structure, that leads to a polarization of Al³⁺ or Mg²⁺ ions to adjacent oxygen lattices, the lattice cell parameter of spinel structure regularly varied with chemical compositions, producing a contraction or expansion effect in the lattice cell, that strongly affects De-SO_x activity. TG analysis showed that during SO₂ oxidative adsorption, most of sulfur species were captured on the surface and some sulfur species were stored in bulk of the solids. The IR and AES results confirmed that both surface and bulk-like sulfates with different H₂-reducibilities were formed on the catalysts, which is in good agreement with results of SO₂ monolayer adsorption measurement. Ten-cycle tests of SO₂ oxidative adsorption and reductive decomposition of the formed sulfate showed that the sample with X_{Al} = 0.33 is the optimum catalyst, its SO₂ capturing capacity reached 124.4 mg/g.

© 2002 Elsevier Science B.V. All rights reserved.

Keywords: Magnesium-aluminate spinel; Sulfur-transfer catalyst; Sulfur-storage capacity; SO₂ emission control; FCC unit

1. Introduction

In the feedstock of fluid catalytic cracking (FCC) process, there exist many different types of sulfur-containing organic compounds, those may poison FCC catalysts, reduce product quality and cause environmental problems. Since 1996, the importance of resid

cracking in FCC operation had become quite apparent, indicating a shortage of high quality crude oil with low content of sulfur on a global scale [1,2]. When the feedstock containing organic sulfur is fed into the FCC units without pretreatment, about 45–55% of the total sulfur compounds present in the feed are converted into hydrogen sulfur during the FCC procedure and 35–45% are still remained in the liquid products, the rest is deposited in the coke formed on the FCC catalysts [3]. The sulfur deposits in the coke are transferred to SO_x (more than 90% SO₂ and less than 10%

* Corresponding author. Tel.: +52-5-7296000x55124; fax: +52-5-5862728.
E-mail address: jwang@ipn.mx (J.A. Wang).

SO₃) when these coke is combusted in the regenerator of FCC units. Nowadays, these SO_x emissions are released out into the air without further treatment in many countries, causing big environmental problems such as acid rain.

Refiners presently have three strategies for controlling FCC SO_x emissions: feedstock pretreatment, flue gas scrubbing and catalyst technology. In the last decade, although many efforts were devoted to hydrodesulfurization (HDS) before FCC process or to flue gas treatment (FGT) after the FCC operation, those would remove most of organic sulfur compounds from FCC feedstock or SO_x from flue emissions of the regenerator, however, because of big cost mainly due to expensive equipment and operations, many refineries so far have not applied HDS or FGT technologies yet.

An interesting technique for SO_x emission control in the FCC units, so-called sulfur-transfer technique, has attracted much attention. A number of patents and scientific articles focusing SO_x abatement in the regenerator in the FCC units by using sulfur-transfer method have been reported [4–8]. This is to use a co-catalyst like magnesium-aluminate spinel material to mix with FCC catalysts for picking-up SO_x produced in the regenerator and then release those sulfur species from the De-SO_x additives in a form of hydrogen sulfide in the reactor and stripper. These H₂S are discharged from the FCC units and separated from the products for further treatment in a modified Claus process, producing elemental sulfur. Because this technique realizes sulfur transferring from SO_x to a useful elemental sulfur, it is therefore called as sulfur-transfer technique, and because the De-SO_x procedure is carried out within the FCC units, this technique is also regarded as “in situ” SO_x control. It has several attractive characteristics: (1) little or no capital investment is required; (2) operation cost is very low, which is only one-seventh or one-thirtieth of the cost used in HDS or FGT; (3) reliability is high, equal to that of the FCC itself; and (4) waste disposal problems are minimal [9,10].

Magnesium-aluminate spinel materials have been commercially used as a sulfur-transfer catalyst in FCC units. However, to develop new generation of the sulfur-transfer catalyst, studies toward improvement of catalytic activity of magnesium-aluminate spinel never cease, most of those focus on structural modifi-

cation by introducing guest ions like iron, copper and cerium, into a stoichiometric magnesium-aluminate spinel to improve its De-SO_x activity [3,7,11–15].

In fact, the crystalline structure of stoichiometric magnesium-aluminate spinel can also be modified by changing Al/Mg mole ratio in the preparation stage. In the stoichiometric MgAl₂O₄ spinel structure, there are eight molecules in its unit cell with 64 tetrahedral symmetry sites and 32 octahedral ones. In the perfect case, magnesium ions occupy eight tetrahedral positions and aluminum ions occupy 16 octahedral positions. In the case of magnesium or aluminum-rich, various magnesium-aluminate solid solution spinels with a formula such as MgAl₂O₄·*n*MgO or MgAl₂O₄·*m*Al₂O₃ can be formed. The excess aluminum ions, for instance, may occupy the positions of magnesium ions, causing spinel structural distortion. The investigation towards relationship between crystalline structure of non-stoichiometric magnesium-aluminate spinel and its De-SO_x catalytic activity is an interesting topic. It was reported that De-SO_x activity of the Mg–Al–O catalysts varied with the Mg/Al mole ratio, and magnesium-rich samples are superior to the aluminum-rich ones [16]. However, whether the bulk structure of the sample involves in the SO₂ adsorption and what kinds of sulfur species are formed on the catalysts is still a matter of debate.

With an emphasis of effects of ratio of alumina to magnesia upon the crystalline structure and thus De-SO_x catalytic activities as well as distribution of the sulfur species from the surface to inner layer of the samples, herein, we report the experiments concerning SO₂ pickup capacity of magnesium-aluminate solid solution spinels, aiming at establishing relationship between De-SO_x activity, reducibility of the formed sulfate and crystalline structures of these catalysts.

2. Experimental

2.1. Catalysts preparation

By using coprecipitation method, a series of catalysts with different chemical compositions were prepared by altering mole ratio of aluminum to magnesium with Mg(NO₃)₂·6H₂O and NaAlO₂ as precursors. As exemplified with stoichiometric

magnesium-aluminate spinel, two solutions were respectively prepared by adding 76.8 g $\text{Mg}(\text{NO}_3)_2 \cdot 6\text{H}_2\text{O}$ and 42.0 g NaAlO_2 . At a same rate, these solutions were slowly added into a 2000 ml-container containing 500 ml of deionized water. During the addition, the formed slurry was stirred and pH value was adjusted at about 9 by using a concentrated nitric acid solution or 2N NaOH solution. Afterwards, the slurry was continuously stirred for an hour and then aged at room temperature over night. The aged slurry was filtered and washed with deionized water. The filtered cake was dried at 120 °C for 10 h and then calcined at 800 °C for 4 h in a furnace in air. The product was ground and the fine materials with 80–160 mesh were used in the SO_2 picking-up experiments.

2.2. Specific surface area measurements

The specific surface areas of the catalyst samples were measured by using liquid nitrogen adsorption method (BET) on an ASAP-2400 apparatus. Before the adsorption the samples were thermally treated at 300 °C for 1 h to eliminate adsorbed species.

2.3. X-ray diffraction analysis (XRD)

X-ray diffraction analysis of the samples were performed on a Rigaku D-max/III B with Cu $\text{K}\alpha$ radiation. Intensity data were obtained in the 2θ range between 10 and 70°. All the XRD data were corrected by using silica as standard sample and therefore the height displacement effect was eliminated. The lattice cell parameter was calculated in virtue of the diffraction line appearing at about 44.0–46.0° which corresponds to (400) plane of spinel crystal, according to the following expression:

$$a = (h^2 + k^2 + l^2)^{1/2} \times d_{hkl} \quad (1)$$

where a is lattice constant (Å), and d_{hkl} is the distance between the (hkl) planes.

2.4. Infrared (IR) characterization

IR in situ measurements were carried out on a HITACHI-270-30 IR spectrometer at different temperatures under vacuum conditions. The adsorption cell is an H-type quartz tube with KBr windows. This adsorption–desorption system was on line with a vacuum set, which was combined two mechanic pumps

and a two-stage oil diffuse pump. Before adsorption operation, the sample was heated in the adsorption cell for 2 h at 300 °C with evacuation. In the case of SO_2 oxidative adsorption, a mixture of 500 Pa of SO_2 and 200 Pa of O_2 was fed into the IR adsorption system for 30 min. In the half cycle of reduction procedure, the sulfated sample was reduced by 500 Pa H_2 at a desired temperature for 10 min.

2.5. SO_2 adsorption and sulfate reduction measurements

De- SO_2 activity measurements were carried out on a MR–GC–MS system. The reactor was a 1.5 cm o.d. quartz tube which was placed in a single-zone furnace controlled by a temperature-programmed system (Model YCC-16). Two chromel–alumel thermocouples encapsulated in a 3 mm o.d. stainless steel sheath, were positioned 1 cm below the top of catalyst bed to measure the temperatures. The 1 g of FCC catalysts (supplied by China Jinling Petrochemical Cooperation) mixing with 3 wt.% De- SO_2 catalyst were heated at 700 °C under a flue of N_2 for 20 min and then 5 vol.% O_2 in N_2 was introduced into the reactor for 5 min. A gaseous mixture containing 1.5 vol.% SO_2 , 5 vol.% O_2 in N_2 was fed at 700 °C for adsorbing 30 min at the rate of 100 ml/min. In the reduction half cycle, the temperature was 500 °C and the reduction time was 10 min; 30 vol.% H_2 in nitrogen was used as reduction gas with a flue rate of 50 ml/min. The catalyst De- SO_2 activity was defined as the conversion of SO_2 . The error of the experimental data reported in Table 3 is 0.1%. Since we want to focus our interest on study of SO_2 adsorption and reduction capacity, the adsorption and reduction time used in the experiments are set longer in comparison with that of the industrial FCC process.

2.6. Auger electron spectroscopy analysis (AES)

Auger electron spectroscopy analysis was performed in a commercial system (Model PHI550-ESCA/SAE) equipped with a 5 keV integral electron gun and a 1 keV sputter-ion gun. All the measurements were made under the following conditions: beam current, $I_a = 1 \mu\text{A}$; primary energy, $I_p = 3 \text{keV}$; modulation voltage, $V_{\text{mod}} = 3 \text{V}$; time constant: $R_c = 0.03 \text{s}$ and the base pressure was about $1.30 \times 10^{-7} \text{Pa}$.

By using the 5 keV integral electron gun and 1 keV sputter-ion gun, it is possible to analyze elemental compositions of the samples from surface to the subsurface. The etching rate of argon ion beam is 70–80 Å/min. Elemental compositions of the samples, in at.%, were determined by using the elemental sensitivity factor method with the following formula:

$$C_x = \frac{I_x/S_x}{\sum I_x/S_x} \quad (2)$$

where C_x is atomic fraction of the element x in the sample, I_x the normalized AES peak height for element x ; S_x the sensitivity factor of element x and Σ is the sum of all the elements present in the sample. The data in Figs. 6 and 7 obtained by this technique are the average of three measurements by choosing different particles.

2.7. Thermogravimetric analysis (TGA) of SO_2 adsorption–desorption

A WRT-2 thermogravimetric analyzer, connected with a computer, temperature-programmed control and vacuum treatment system, was used to measure the weight changes of the sample during the adsorption and reduction processes (Fig. 1). Generally, 10–15 mg sample was placed in a quartz sample pan. The standard experimental conditions of SO_2 adsorption and H_2 -reduction of the sulfated samples are

Table 1
Standard experimental condition in TGA for SO_2 adsorption and reduction

	SO_2 oxidative adsorption	Sulfur species reduction
Temperature ($^{\circ}\text{C}$)	700	500
Gases mixture	1.2 vol.% SO_2 , 20 vol.% O_2	30 vol.% H_2
Balance gas	N_2	N_2
Time (min)	30	10
Flow rate (ml/min)	100	50

reported in Table 1. The standard error measured by WRT-2 thermogravimetric analyzer is 0.1 mg.

3. Results and discussion

3.1. Crystalline structures and phase domains of the samples

The XRD diffraction patterns of the samples with various alumina mole fractions between 0.75 and 0.33 show a single phase corresponding to magnesium-aluminate spinel. All the XRD spectra are very similar but with a shift of the peak position as the alumina mole fraction is changed. Fig. 2 shows the XRD pattern of the sample with alumina mole fraction $X_{\text{Al}} = 0.7$. The three strong diffraction peaks corresponding to the (3 1 1), (4 0 0) and (4 4 0) planes of

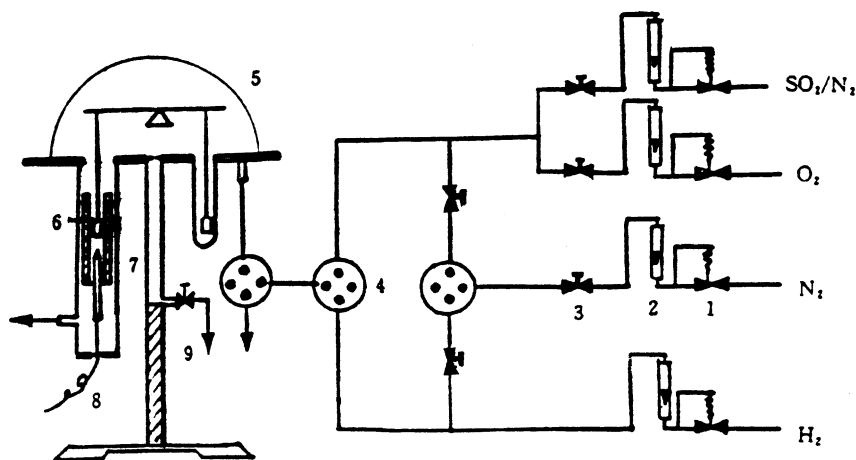


Fig. 1. A microbalance analysis system for SO_2 adsorption and reduction measurements (1) needle valve; (2) flow meter; (3) stop valve; (4) six-way valve; (5) microbalance house; (6) sample holder; (7) furnace; (8) thermocouple; (9) vacuum system.

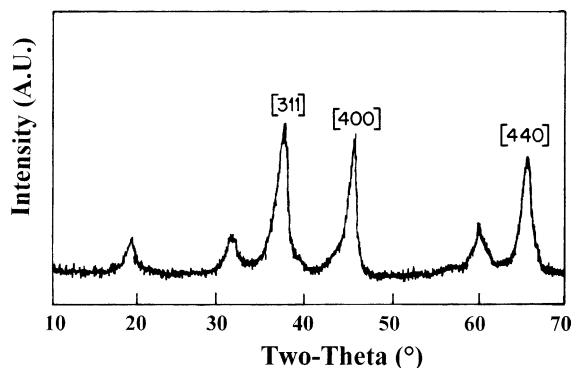


Fig. 2. XRD pattern of the sample ($X_{\text{Al}} = 0.7$) calcined at 800 °C for 4 h. Only magnesium-aluminate spinel phase is formed.

a magnesium-aluminate spinel crystal, were clearly observed, indicating the sample was well crystallized when they were calcined at 800 °C. However, the diffraction line shifts with changing of alumina mole fraction. Table 2 gives two-theta data of the diffraction line registered between 44.0 and 46.0°, which corresponds to a value of d -spacing varying from 1.995 to 2.034 Å. When the alumina mole fraction was very small ($X_{\text{Al}} < 0.33$), two phases MgAl_2O_4 and MgO coexisted (Fig. 3).

The formation of magnesium-aluminate spinel with various compositions can be generally illustrated as follows:

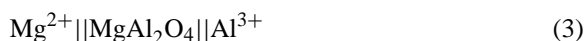


Table 2

Data of alumina mole fraction (X_{Al}), two-theta, d -spacing, lattice cell parameter a and SO_2 conversion of magnesium-aluminate spinels

X_{Al}	2θ (°)	d_{400} (Å)	Cell parameter a (Å)	SO_2 conversion (%)
0.91	45.52	1.995	7.981	58.6
0.89	45.40	2.000	8.000	
0.86	45.24	2.007	8.030	60.5
0.80	45.22	2.008	8.032	61.3
0.75	45.18	2.009	8.036	
0.70	45.20	2.009	8.035	65.2
0.60	45.06	2.015	8.059	68.6
0.50	44.94	2.021	8.080	71.7
0.40	44.76	2.028	8.112	73.1
0.33	44.62	2.034	8.134	74.3
0.25	44.88	2.023	8.089	
0.20	44.92	2.020	8.082	70.0

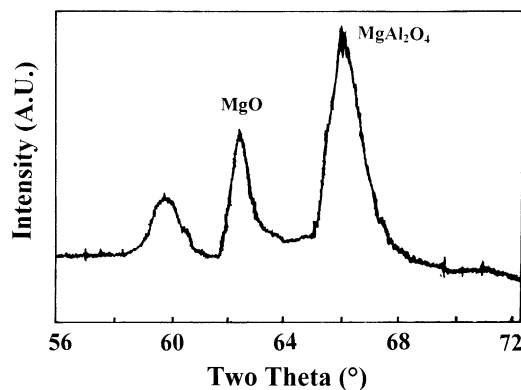


Fig. 3. XRD pattern of a magnesium-rich sample ($X_{\text{Al}} = 0.2$) calcined at 800 for 4 h. This sample contains a MgO phase and magnesium-aluminate spinel phase.

where “||” is the boundaries between magnesium-aluminate spinel crystals and precursor cationic ions. During synthesis process, many fine crystal cores of magnesium-aluminate spinel surrounded by many magnesium and aluminum ions can be formed in the solid mixture. Above 600 °C, growth of these fine crystal cores is rapid since the reactions of spinel formation occur on the boundaries or interfaces of these crystals [17–21].

It is assumed that the formation of solid spinel is a result of Mg^{2+} or Al^{3+} ions diffusing into the deficient spinel-type structure of γ -alumina ($\text{Al}_{8/3}\text{O}_4$). Therefore, the formula of solid solution can be written as $\text{Mg}_x\text{Al}_{(8-2x)/3}\text{O}_4$ [18]. The stoichiometric spinel corresponds to $x = 1$, i.e. MgAl_2O_4 . The lowest possible limit is $x = 0$ and that corresponds to γ - Al_2O_3 ; the highest possible limit is $x = 4$, corresponding to pure MgO (Mg_4O_4). In the above formula, x is the MgO mole number, while, the Al_2O_3 mole number (y) is equal to $(8 - 2x)/6$ that is half of aluminum mole in the formula of $\text{Mg}_x\text{Al}_{(8-2x)/3}\text{O}_4$. Thus, the mole fraction of alumina (Al_2O_3), X_{Al} can be expressed as

$$X_{\text{Al}} = \frac{y}{x + y} = \frac{(8 - 2x)/6}{((8 - 2x)/6) + x} = \frac{8 - 2x}{8 + 4x} \quad (4)$$

The lattice cell parameter (a) obtained from XRD analysis, as a function of alumina mole fraction X_{Al} , is reported in Table 2 and plotted in Fig. 4. It is found that the samples have different limited domains of the composition on both sides of stoichiometric spinel.

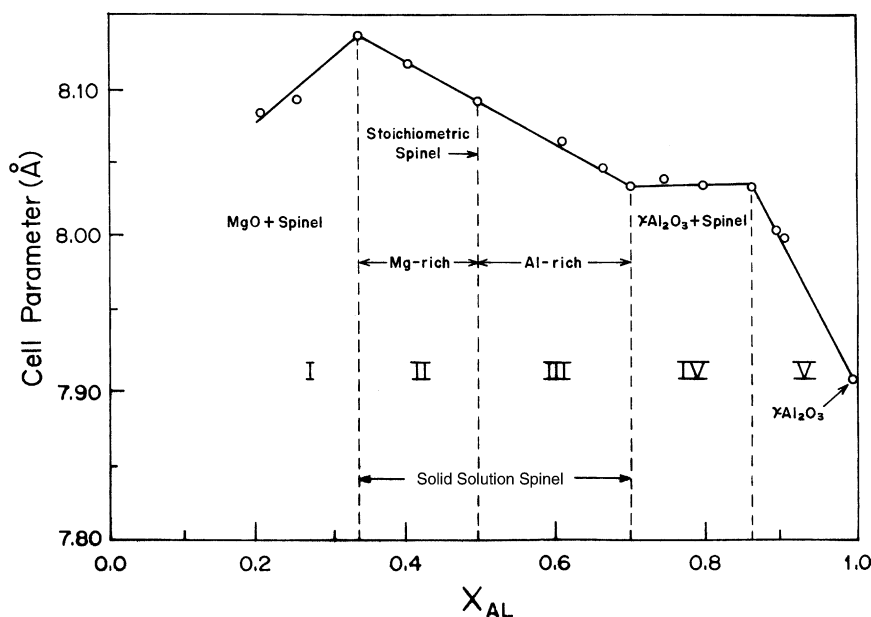


Fig. 4. Lattice constants of the samples as function of alumina mole fraction.

When $X_{Al} > 0.5$, the domains corresponded to a deficient spinel since the total number of cations was lower than 3. When $X_{Al} < 0.5$, the domain was related to a magnesium-aluminate solid solution spinel in which magnesium ion was excess because the total number of cations was bigger than 3.

In the domains II and III, where X_{Al} was between 0.33 and 0.70, the cell parameter a lineally increased from 8.032 to 8.134 Å as alumina mole fraction decreased. However, in domain IV ($0.70 < X_{Al} < 0.86$), the cell parameter a remained almost unchanged. When alumina content is very high ($X_{Al} > 0.86$), the cell parameter closely pointed to the value of the lattice parameter of γ - Al_2O_3 (domain V). In the case of magnesium very rich ($X_{Al} < 0.33$), however, the cell parameter tended toward the value of the stoichiometric spinel (domain I).

As it is well known that in crystals there exists ionic polarization effect, which is mainly determined by two factors: (i) ion radius and (ii) ion charges. This polarization can alter the distance between a cationic ion and its neighbor anion in the crystalline structure by producing interaction between them and thus the lattice cell parameter. In the magnesia–alumina system, the polarizing power of Al^{3+} and Mg^{2+} to its adja-

cent oxygen is different, this results in the lattice cell parameter regularly changing with composition. For Al^{3+} ions, the value of positive charge is high and its radius is small ($r_{Al^{3+}} = 0.0675$ nm), its polarizing power to the adjacent oxygen ion is therefore strong. In the case of aluminum-rich, the excess Al^{3+} ions would diffuse into the lattice cell of $MgAl_2O_4$ and occupied some Mg^{2+} vacancies. The strong polarization to adjacent oxygen ion shortened the distance between cationic and adjacent oxygen ions, leading to a contraction of lattice cell.

On the other hand, compared with Al^{3+} ion, the positively charged Mg^{2+} ion shows lower chemical valence and larger ion radius ($r_{Mg^{2+}} = 0.071$ nm), hence, the ability of Mg^{2+} polarizing to oxygen ions is relatively weaker in comparison with aluminum ion. In the magnesium-rich case, these excess Mg^{2+} ions migrated into the lattice cell and occupied aluminum vacancies or lattice positions, expanding the cell volume. The maximum value of lattice parameter a corresponding to $MgAl_2O_4$ · MgO is probably a result of the largest expansion of the lattice cell caused by the strongest polarization due to the maximum substitution of aluminum by magnesium ions. This reasonably interprets the tendency of cell parameter

changing with chemical composition on both sides of stoichiometric spinel within the domains II and III.

Free MgO phase can be segregated from the magnesium-aluminate spinel in the case of magnesium very rich. When X_{Al} was less than 0.33 (domain I), a new peak corresponding to magnesia phase appeared at around 62.4° , showing that free MgO and spinel phases coexisted in the sample (Fig. 3). MgO formation diminishes the replacement of aluminum ions by magnesium ions in the structure of $MgAl_2O_4$, leading to the lattice parameter of magnesium-aluminate spinel close to the value of the lattice parameter corresponding to stoichiometric spinel.

It is noted that in domain IV, the cell parameter remained almost unaffected when alumina mole fraction changed. Though we could not find a satisfactory explanation for this result, it is assumed that magnesium-aluminate spinel coexisted with γ -alumina in this domain. Since the crystalline structure of magnesium-aluminate spinel and γ -alumina have the same atomic coordinates, their XRD patterns are very similar, that produces difficulty to strictly distinguish the difference between them. However, change of the lattice cell parameter reflects its structural modification or distortion. In this region, a slight increase in magnesium content might only cause an increase in amount of magnesium-aluminate spinel. This is because in the aluminum-rich case, magnesium ions can be consumed by reacting with the excess aluminum ions to form more magnesium-aluminate spinel, which, of course, is deficient. It may be more deficient than that in domain III but less than that in domain V. The cell parameter is a result of contributions of formation of both alumina and $MgAl_2O_4$ spinel as well as each weight fraction, that finally leads to the parameter remaining almost constant.

In the domain V ($0.86 < X_{Al} < 1.0$), aluminum content is very high. It is probably in favor of the formation of the spinel having a very deficient structure similar to γ -alumina. Therefore, the cell parameter decreases with the increasing of alumina mole fraction and it points toward the value of γ -alumina. Or, similar to the explanation for the domain IV, it might be also interpreted by assuming coexistence of magnesium-aluminate spinel and γ -alumina in this domain. Since γ -alumina is the dominant phase, it results in lattice parameter linearly diminishing with increasing of alumina mole fraction.

3.2. De-SO₂ activity and H₂ reducibility

An ideal sulfur-transfer catalyst is the one on which the formed sulfates are thermally stable under the regeneration condition but are easily reduced under the reaction condition in FCC process. Thermal non-stability of the sulfate formed on the De-SO₂ catalysts usually results in occurrence of the reversible reaction of sulfate formation, as in the case of alumina used as additives, where SO₂ is produced from the decomposition of $Al_2(SO_4)_3$ at temperature $700^\circ C$ in the regeneration condition of FCC units. The sulfate formed on magnesium-aluminate spinel has been proved to be stable at $700^\circ C$ [22]. However, if sulfates can not be easily removed from the De-SO₂ additives in the riser reactor and stripper, the active sites for capturing SO_x may be partially lost and this must shorten lift-time of the catalysts. Therefore, it is important for a high quality sulfur-transfer catalyst that its SO₂ oxidative adsorption ability must match to reducibility of the formed sulfate during the FCC cycles. In order to measure such a compatibility of different spinel-type catalysts, 10-time cycles of SO₂ oxidative adsorption and reductive desorption were carried out. The SO₂ conversions on different catalysts are reported in Tables 2 and 3.

It is observed from the Tables 2 and 3 that the De-SO₂ activities of aluminum-rich samples are lower than that of magnesium-rich samples. However, when the samples were very rich magnesium ($X_{Al} < 0.33$) not only De-SO₂ activities but also mechanical

Table 3

De-SO₂ activities of 10 cycles of SO₂ adsorption and reduction of formed sulfur species on the different magnesium-aluminate spinels measured by using microreactor system

No. of the reduction–oxidation cycle	Captured SO ₂ (%)		
	$X_{Al} = 0.5$	$X_{Al} = 0.33$	$X_{Al} = 0.8$
1	71.7	74.3	61.3
2	68.2	70.8	57.4
3	68.7	70.2	60.2
4	69.1	69.3	56.3
5	67.4	70.8	55.9
6	66.0	68.8	57.6
7	68.2	68.4	58.0
8	65.1	70.5	56.4
9	63.1	70.4	56.1
10	62.9	71.5	55.8

strength became poor that would reduce the ability of attrition resistance. Therefore, a suitable content of magnesium in spinel is an important factor in the design of De-SO_x catalysts.

All the samples showed relatively high initial activities. After two cycles of adsorption–reduction operation, the De-SO_x activities of the catalyst samples decreased; then they almost remained at constant after eight cycles. This is because many active sites exist on the fresh surfaces, after several cycles of SO₂ adsorption, part of formed sulfate species still remained on the surface or subsurface, poisoning some of active sites and thus resulting in partial deactivation. For the best catalyst, MgAl₂O₄·MgO ($X_{Al} = 0.33$), there was only an approximate 2.8% loss of the activity in the 10th oxidation–reduction cycle compared with the fresh sample.

The abilities of SO₂ pickup under a fixed temperature 700 °C and reducibility at 500 °C of the different catalysts were also measured by using microbalance technique (Table 4). The data in Table 4 show that the sample with $X_{Al} = 0.33$ is the most active sulfur-capturing catalyst, its SO₂-capturing capacity reaches 124.4 mg/g. This result is also in consistent with the results obtained from microreactor test shown in Table 3.

When being reduced by hydrogen, the sulfated samples show some weight loss. The reducing factor, W_r/W_i , ranges from 0.958 to 0.992. It seems from W_r/W_i values that reducibilities of the samples are quite good. However, the desorption of lattice oxygen on the surface of the samples due to the reaction between lattice oxygen and hydrogen to form water,

which also causes weight loss, should be taken into account when we evaluate the reducibility. Since the values of W_r/W_i for all the samples are less than 1, and after consideration of the weight loss resulting from the lattice oxygen desorption, we conclude that some adsorbed sulfur species are still retained in the samples after reduction with hydrogen.

3.3. Capacity of SO₂ monolayer adsorption and bulk-storage

The total amount of sulfur dioxide adsorbed on the catalyst sample could be measured by microbalance technique as shown above. However, it is interesting to know how many SO₂ were captured on the catalyst surface. The cross sectional area of SO₂ molecules is estimated to be 0.1 m²/μmol [23–25]. For calculation the amount of SO₂ monolayer adsorption on the catalyst surface, we assumed that each adsorbed sulfur dioxide molecule close two-dimensional packing covers an area that is equal to the value of cross-sectional area of single SO₂ molecule (S_s). According to surface area of the sample and value of S_s , the amount of SO₂ adsorbed in a monolayer on the sample surface was calculated (Table 5). It is clearly shown for all the tested samples that the total amount of adsorbed SO₂ is more than that corresponding to a monolayer.

Three possible reasons are responsible for the extra-adsorbed species: (i) the adsorbed oxygen species since it is a oxidation adsorption process; (ii) multi-layer adsorbed SO₂ on the surface and (iii) SO₂ storing in the inner layer of the sample.

For testing the first possibility, we used pure oxygen as adsorbent to measure weight gain of the samples

Table 4

Data of SO₂ oxidative adsorption and reduction of the sulfur species formed on the different catalysts obtained by using TGA technique^a

X_{Al}	W_i (mg)	W_a (mg)	W_r (mg)	W_r/W_i	$\Delta W/W_i$ (mg/g)
0.86	11.44	12.38	11.25	0.983	82.5
0.70	10.11	11.04	9.87	0.976	92.0
0.50	14.80	16.25	14.34	0.969	98.0
0.33	10.05	11.30	9.97	0.992	124.4
0.20	12.39	13.73	12.94	0.958	108.2

^a W_i : initial weight of the fresh sample; W_a : weight of the sulfated sample at 700 °C; W_r : weight of the reduced samples at 500 °C; W_r/W_i : reducing factor, $\Delta W = W_a - W_i$; $\Delta W/W_i$: capacity of SO₂ pickup.

Table 5

Amount of SO₂ monolayer adsorption and storage capacity of SO₂ in bulk of the different samples^a

X_{Al}	S (m ² /g)	W_m (mg/g)	W_o (mg/g)	W_e (mg/g)	W_s (mg/g)
0.86	116.9	74.8	1.6	7.7	6.1
0.70	132.6	84.9	2.4	7.1	4.7
0.50	147.1	94.1	3.3	13.9	10.6
0.33	169.2	108.3	2.7	16.1	13.4
0.20	151.6	97.1	0.9	11.8	10.9

^a S : Specific surface area; W_m : amount of monolayer adsorbed SO₂; W_o : amount of adsorbed oxygen; W_e : amount of the extra weight gain, $W_e = W_a - W_m$; W_s : amount of SO₂ storing in the bulk of the sample, $W_s = W_e - W_o$.

in the same condition as SO₂ oxidative adsorption. It was found that weight gain for all of the samples is less than 3.5 mg/g. These results indicate that oxygen adsorption may be responsible for part of the extra weight gain when the samples adsorb SO₂ in the presence of oxygen. The data regarding oxygen adsorption are also reported in Table 5. However, it is noteworthy that SO₂ adsorption procedure is an oxidation adsorption process, the adsorbed oxygen may oxidize the adsorbed SO₂ to SO₃ and form sulfate, for example, when SO₂ adsorbs on Mg²⁺, MgSO₄ may be formed based on the Eqs. (5) and (6):



Therefore, the adsorbed oxygen had been taken into account when we measured the weight gain during SO₂ oxidative adsorption. The amount of adsorbed oxygen molecules, which are not involved in sulfate formation at 700 °C, is very small. Its existence does not produce significant effect on weight gain.

The second possibility is generally exclusive since it conflicts with our adsorption experiments where the

temperature is as high as 700 °C. Existence of multi-layer SO₂ is only possible in the low temperature due to very weak bond between the absorbents.

After getting rid of the first two possibilities, it is postulated that the extra weight gain (W_e) was caused by the storage of SO₂ in some form in inner layer of the samples. Capacity of SO₂ storage in the bulk in each sample is presented in Table 5.

The data in Tables 4 and 5 show that most sulfur species were adsorbed on the surface of samples and less than 15 wt.% of sulfur adsorbed species were “stored” in bulk. Also it was found that SO₂ storage capacity in magnesium-rich sample ($X_{\text{Al}} = 0.2$) is higher than that in aluminum-rich samples ($X_{\text{Al}} = 0.7$ and 0.86). The sample with $X_{\text{Al}} = 0.33$ had the largest ability to store the SO₂ in the bulk, which might be related to its special structure, since this sample has the biggest lattice cell volume and the largest surface area (169.2 m²/g). Moreover, SO₂ adsorption on base magnesium-aluminate spinel may be an acidic–basic reaction process, its capacity may also associate to basicity and surface area of the solids. A plot concerning the relationship among the SO₂ adsorption capacity, catalyst basicity and surface area is shown in Fig. 5.

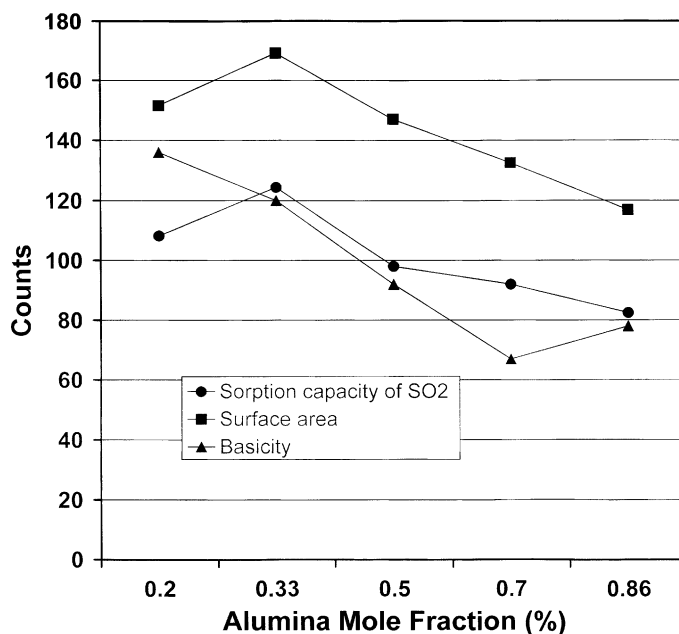


Fig. 5. Sorption capacity for SO₂, basicity and surface area of the catalysts as function of alumina mole fraction. Sorption capacity of SO₂, mg/g; surface area, m²/g; basicity, CO₂ μmol/g × 10⁻¹.

It is found that both sorption capacity for SO_2 and surface area first increases as alumina mole fraction increases from 0.2 to 0.33, and then dramatically decrease as X_{Al} declining to 0.86. However, the change tendency of the basicity as function of X_{Al} follows some different way, indicating that SO_2 oxidative adsorption is not a strict base–acid reaction. These results show that the capacity of SO_2 picking-up of the catalysts is closely related to not only Al/Mg composition but also surface area.

3.4. Distribution of sulfur species in depth along the catalyst particles

AES technique was applied to measure the sulfur species distribution in depths in the samples by using argon ion as sputter gun. Sulfur atom concentrations in the samples as a function of Ar^+ sputter time that is proportional to depth of the particle, are shown in Figs. 6 and 7, respectively.

Sulfur atom concentration in the sulfated samples reached a top value on the surface and then it decreased from the outer to inner layer (Fig. 6). After being reduced by H_2 at 500°C , some residual sulfur species located at different depths were still observed (Fig. 7). On the surface and subsurface, all the sulfur species

are completely removed, while, as the sputter time increased, the sulfur concentration gradually increased, and at 200–210 Å (after 3 min of Ar^+ etching), a maximum value was achieved, and then sulfur concentration diminished with the increment of depth. These results show that sulfur species formed on surface or subsurface can be easily removed, however, reduction of the sulfur species in the bulk is more difficult.

The maximum value of the residual sulfur species in the depth range of 200–210 Å is likely caused by comprehensive reasons: on the one hand, the amount of SO_2 adsorption decreased as the depth increased, and in the interior region, which may be near the center of particle, it was much less; on the other hand, reduction of the sulfur species on the surface was easier than that on the inner surface. Consequently, after reduction by hydrogen, on the surface and the inner layer at greater depth, the amount of residual sulfur species was less than that presenting in the range of 200–210 Å depth.

3.5. Formation of surface sulfate and bulk-like sulfate

Although both microbalance and AES analysis confirm sulfur species being stored in the bulk or

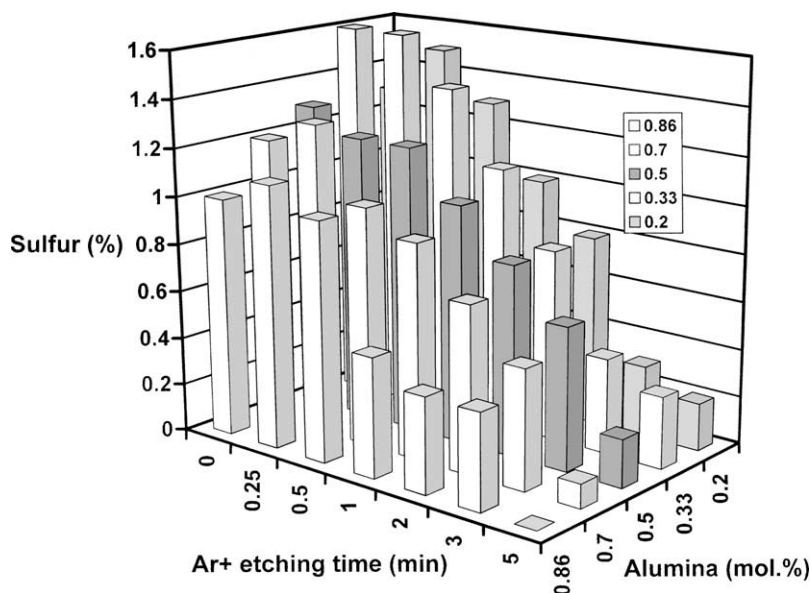


Fig. 6. Sulfur content as a function of Ar^+ sputter time for the various sulfated samples.

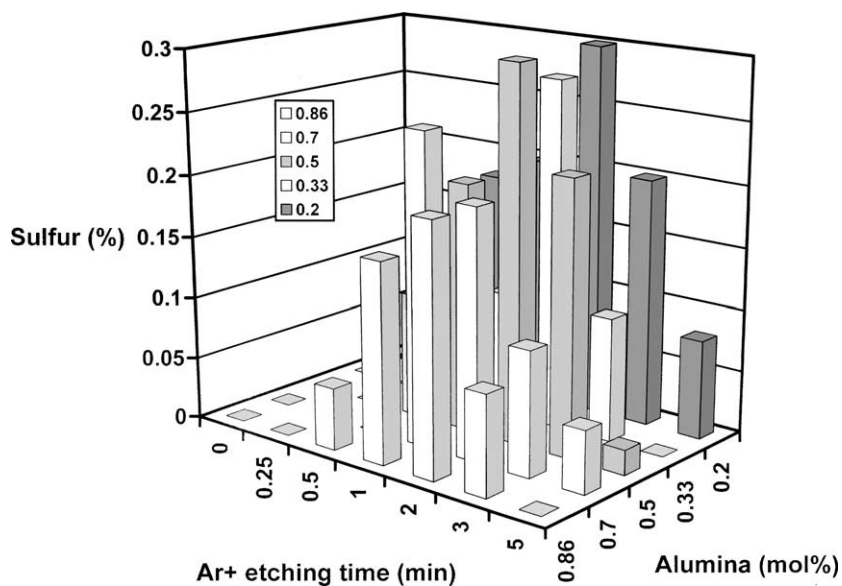


Fig. 7. Sulfur content as a function of Ar⁺ sputter time for the various reduced samples.

inner layer of the samples, however, some questions naturally arise: in which form the sulfur species were stored in the surface or bulk and how about their thermal stability and H₂-reducibility? To investigate this, the sample with $X_{Al} = 0.33$ was characterized by in situ IR technique (Fig. 8). Five absorption bands were observed when the sample was exposed in the mixture of SO₂ and O₂ in the IR adsorption cell at 500 °C for adsorption 30 min. These bands, respectively appeared at 1400, 1300, 1190, 1075 and 950 cm⁻¹. After 60 min of adsorption, the IR spectra remained unchanged, indicating that the adsorption on this sample reached saturation under this condition. The band at 1300 cm⁻¹ rapidly disappeared when the adsorption system was evacuated up to 5 Pa, however, the intensities of other bands remained more or less unaffected (not shown here). This reveals that the band at 1300 cm⁻¹ was produced by weakly adsorbed sulfur species. With respect to thermal stability, the bands at 1400, 1075, 1190 and 950 cm⁻¹ are assigned to the strong bounded sulfur species on the samples.

Various sulfur bands formed on different oxides exposed under SO₂ atmosphere have been reported. Datta et al. observed five different sulfur species formed on the γ -Al₂O₃: 1334 and 1148 cm⁻¹ (physically adsorbed species on OH groups); 1322

and 1140 cm⁻¹ (weakly chemisorbed); 1255 and 1189 cm⁻¹ (chemisorbed on acidic sites) and 1060 cm⁻¹ (strong chemisorbed species) [26]. Waqif et al. observed an intense IR absorption band in the region 1100–1200 cm⁻¹ on magnesium-aluminate spinel sample and it was ascribed to bulk or ion-like sulfate [22]. Similarly, bulk-like sulfate was found on MgO and γ -Al₂O₃ samples during SO₂ oxidative adsorption [25,27]. Referring to IR character of the sample impregnated with ammonia sulfate [28–30], the above bands were assigned to asymmetric (ν_a) and symmetric (ν_s) O=S=O and O–S–O stretching vibration of surface and bulk-like sulfates. It is reasonable that during adsorption, SO₂ weakly adsorbed on some active sites as physical adsorption species on the one hand and strongly bounded sulfur-species reacted with oxygen lattices of the catalysts to form surface sulfate or bulk-like sulfate on the other hand [24]. The formation of bulk-like sulfate MgSO₄ on magnesium-aluminate spinel is also confirmed by XRD analysis [3,7]. We here therefore, assigned the more thermal stable bands at 1075 and 1190 cm⁻¹ to bulk-like sulfates.

It was reported that when the sulfur complexes can be formed through O– or S–metal bond, depending on the value of ($\nu_a - \nu_s$): if $\nu_a - \nu_s > 190$ cm⁻¹, it may be

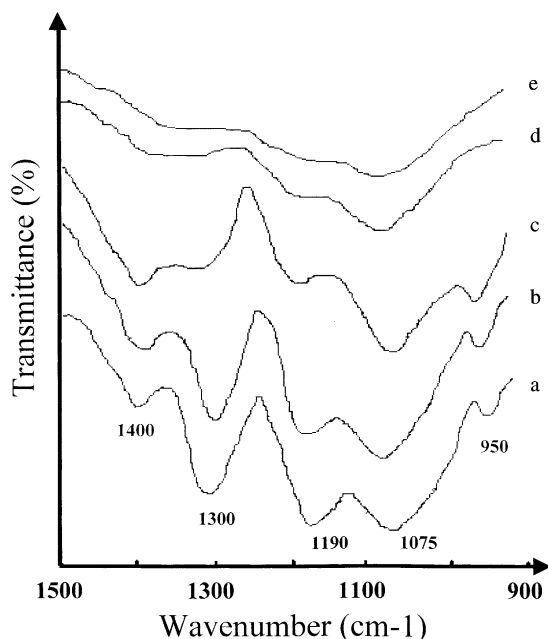


Fig. 8. IR spectra of the sample ($X_{Al} = 0.33$) treated with SO_2 and O_2 and then being reduced with H_2 at different conditions. (a–b) After the sample was exposed in a mixture of 500 Torr SO_2 and 200 Torr O_2 for 30 min at $500^\circ C$ (a) and 60 min (b); (c–e) after the adsorption system was evacuated to 20 Pa at $500^\circ C$, a steam of 500 Torr 100% H_2 was fed into the adsorption cell, IR spectrum was recorded at $500^\circ C$ after the sample being reduced for 3 min (c), 30 min (d) then the temperature was increased up to $600^\circ C$ (e).

O–M bond; however if $\nu_a - \nu_s < 190\text{ cm}^{-1}$, the S–M bond may be formed [26]. Based on these argument, in our cases sulfate species was probably formed via S–M bond since the value of $\nu_a - \nu_s$ was less than 190 cm^{-1} .

When the sulfated sample was treated with hydrogen at $500^\circ C$ for 3 min, all the bands were also remarkably reduced in intensity. After 30 min reduced, both the 1400 and 950 cm^{-1} bands disappeared and the intensities of 1065 and 1200 cm^{-1} bands were further reduced. As the reduction temperature increased to $600^\circ C$, the 1065 and 1200 cm^{-1} bands were almost disappeared. These observations reveal that all surface sulfates could be reductively decomposed at moderate temperature but the bulk-like sulfates, which are only partially removed at the reaction temperature ($500^\circ C$). Fortunately, in the industrial practice, when the De- SO_x catalysts together with FCC cata-

lysts move into the riser reactor of FCC unit, they still remain some temperature between 700 and $500^\circ C$ for a few seconds, this is very important since the bulk-like sulfates can be removed at relatively high temperature during this short residence time. In comparison with stoichiometric magnesium-aluminate spinel, $MgAl_2O_4 \cdot MgO$ has larger SO_2 picking-up capacity and higher ability to reduce the formed sulfate [30].

4. Conclusions

The crystalline structures and De- SO_2 activities of a series of magnesium-aluminate solid solution spinel catalysts were found to be very sensitive to chemical compositions. A lattice cell expansion or contraction, occurring in the structures of magnesium- or aluminum-rich samples, was determined, it was a result of polarization effect of Al^{3+} ions or Mg^{2+} ions to its adjacent lattice oxygen ions in the crystalline structure of $MgAl_2O_4$. The catalytic properties of magnesium- or aluminum-rich catalysts remarkably differed from that of stoichiometric spinel. The similar trends of both of lattice cell parameters and De- SO_2 activity varying with the catalyst composition indicate that the crystalline structure of catalyst is one of the key factors to affect catalytic activity.

SO_2 was captured on all the samples in an amount more than that of a monolayer. The concentration of the sulfur species distributing in depth of the sample decreased from surface to central region. Most of sulfur species were formed on surface, which could be easily removed during hydrogen reduction procedure at $500^\circ C$. However, some of sulfur species was stored in sulfate in the bulk that resisted to H_2 -reduction up to $600^\circ C$. The formation of both surface and bulk-like sulfates on the catalysts enhanced the capacity of SO_2 pickup.

Acknowledgements

J.A. Wang would like to thank the financial support from CONACyT-31282-U (Mexico) and FEIS-98-29-III (IMP-IPN-Mexico) and a scientific advisor fellowship of the Proyect-IMP-D.1234.03.012. L.F. Chen thanks the fellowship of visiting professor supported by the CONACyT and FIES projects

in the Instituto Plitecnico Nacional de Mexico. The technical assistance from Professor H. L. Zhou for the AES analysis and from Ms. Y. F. Chen for the IR experiments is greatly appreciated.

References

- [1] J.P. Verlaan, P. O'Connor, H.W.M. Sonnemans, Y. Inoue, in: Proceedings of the 15th World Petroleum Congress, Beijing, China, 1997, p. 1.
- [2] B.A. Lerner, *Hydrocarbon Eng.* 3 (1998) 26.
- [3] A. Corma, A.E. Palomares, F. Rey, *Appl. Catal. B* 4 (1994) 169.
- [4] R.J. Bertolacinl, E.H. Hirschberg, F.S. Modica, US Patent 4,432,019 (1983).
- [5] J.S. Yoo, F. Lossamoor, J.A. Jaecker, US Patent 4,492,678 (1985).
- [6] L.M. Magnabosco, E.J. Demmel, US Patent 5,108,979 (1992).
- [7] J.S. Yoo, A.A. Bhattachryya, C.A. Radlowski, J.A. Karch, *Ing. Eng. Chem. Res.* 31 (1992) 1252.
- [8] E. Astorino, G. Busca, G. Ramis, R.J. Willey, *Catal. Lett.* 23 (1994) 353.
- [9] F.A. Pettersen, W.A. Blanton, National AIChE Meeting, Session No. 37, 26 August 1986, Boston, MA, USA.
- [10] D.P. MxArthur, H.D. Simpson, K. Baron, *Oil Gas J.* (1983) 70.
- [11] J.S. Yoo, A.A. Bhattacharyya, C.A. Radlowski, *Appl. Catal. B: Environ.* 1 (1992) 169.
- [12] J.A. Wang, L.F. Chen, C.L. Li, *J. Mol. Catal.* 139 (1999) 31.
- [13] J.A. Wang, Z.L. Zhou, C.L. Li, *J. Mol. Catal.* 139 (1999) 315.
- [14] J.A. Wang, O. Novaro, C.L. Li, *J. Mater. Sci.* 33 (1998) 3671.
- [15] J.A. Wang, L.F. Chen, C.L. Li, *React. Kinet. Catal. Letts.* 1 (1998) 73.
- [16] J.S. Yoo, A.A. Bhattacharyya, C.A. Radlowski, *Ind. Eng. Chem. Res.* 30 (1991) 1444.
- [17] O. Salas, H. Ni, V. Jayaram, K.C. Vlach, C.G. Levi, R. Mehrabian, *J. Mater. Res.* 6 (1991) 1964.
- [18] Y.M. Chang, W.D. Kingery, *J. Am. Ceram. Soc.* 72 (1989) 271.
- [19] C.C. Wang, *J. Appl. Phys.* 40 (1969) 3433.
- [20] G. Yamaguchi, M. Nakano, M. Tosaki, *Bull. Chem. Soc. Jpn.* 42 (1969) 2801.
- [21] A. Navrotski, B.A. Wechsler, F. Siefert, *J. Am. Ceram. Soc.* 69 (1986) 418.
- [22] M. Waqif, O. Saur, J.C. Lavalley, Y. Wang, B.C. Morrow, *Appl. Catal.* 71 (1991) 319.
- [23] P.H. Emmett, S. Brunauer, *J. Am. Chem. Soc.* 59 (1937) 1553.
- [24] S.W. Nam, G. Gavalas, *Appl. Catal.* 55 (1989) 193.
- [25] S.W. Nam, G. Gavalas, *Appl. Catal.* 74 (1991) 53.
- [26] A. Datta, R.G. Gavell, R.W. Tower, Z.M. George, *J. Phys. Chem.* 89 (1985) 443.
- [27] M. Bensitel, M. Waqif, O. Saur, J.C. Lavalley, *J. Phys. Chem.* 93 (1989) 6581.
- [28] M. Waqif, O. Saur, J.C. Lavally, G. Centi, *J. Phys. Chem.* 95 (1991) 4051.
- [29] T. Yamaguchi, T. Jin, K. Tanabe, *J. Phys. Chem.* 90 (1986) 3148.
- [30] J.A. Wang, C.L. Li, *Appl. Surf. Sci.* 161 (2000) 406.